Longitudinal Tracking Studies for a High Intensity Proton Synchrotron *

E. Lessner, Y. Cho, K. Harkay, K. Symon†

Argonne National Laboratory
9700 Cass Ave., Argonne, IL 60439

Abstract. Results from longitudinal tracking studies for a high intensity proton synchrotron designed for a 1-MW spallation source are presented. The machine delivers a proton beam of 0.5 mA time-averaged current at a repetition rate of 30 Hz. The accelerator is designed to have radiation levels that allow hands-on-maintenance. However, the high beam intensity causes strong space charge fields whose effects may lead to particle loss and longitudinal instabilities. The space charge fields modify the particle distribution, distort the stable bucket area and reduce the rf linear restoring force. Tracking simulations were conducted to analyze the space charge effects on the dynamics of the injection and acceleration processes and means to circumvent them. The tracking studies led to the establishment of the injected beam parameters and rf voltage program that minimized beam loss and longitudinal instabilities. Similar studies for a 10-GeV synchrotron that uses the 2-GeV synchrotron as its injector are also discussed.

Introduction

Feasibility studies of a proton source for a 1-MW spallation source were performed at Argonne National Laboratory [1]. The machine is designed to deliver a proton beam of 0.5 mA time-averaged current at a repetition rate of 30 Hz. The 1-MW proton source is based on a 2-GeV, 30-Hz rapid cycling synchrotron. A key design feature of the accelerator system is to minimize beam losses during the whole injection to extraction cycle, reducing activation to levels consistent with hands-on maintenance. The time-averaged current in

*Work supported by U. S. Department of Energy, Office of Basic Energy Sciences under Contract No. W-31-109-ENG-38.

†Also Dept. of Physics, University of Wisconsin-Madison, Madison, WI 53706

the synchrotron is 0.5 mA, corresponding to 1.04×10^{14} protons per pulse. This intensity is about two times higher than that of existing machines and causes strong space charge fields that affect the dynamics of the injection, capture and acceleration processes.

The space charge fields modify the particle distribution, distort the stable bucket area, and reduce the rf linear restoring force, causing loss of focussing or even defocussing. These effects may lead to particle loss. Another factor that affects the longitudinal dynamics is the tune depression introduced by the space charge forces. Space charge can potentially lead to collective instabilities which may introduce emittance growth and/or beam loss.

Tracking simulations were conducted to study space-charge-related effects in the accelerator and ways to circumvent them. The results were used to design the injected beam chopping requirements, introduced to facilitate loss-less capture, the injected beam energy spread and an rf voltage program that prevented losses and longitudinal instabilities.

Similar studies were also conducted for the 10-GeV rapid cycling synchrotron of a 5-MW proton source [2]. The 10-GeV synchrotron uses the 2-GeV machine as its injector.

The bucket area reduction due to the space charge is an important consideration in the matching process between the extracted beam from the 2-GeV machine and the waiting bucket of the 10-GeV machine. In this case, neglect of space charge contributions in the matching calculations leads to a badly mismatched beam and consequent dilution as the beam is accelerated.

In the following, we discuss first the relevant features of the simulation code that we developed for the studies. Then, we discuss space-charge-related issues in the 2-GeV synchrotron. Finally, we discuss those issues that are specific to the 10-GeV synchrotron.

Tracking Algorithm

A Monte-Carlo-based tracking computer program was developed to study space charge effects [3][4] and to determine the injected beam parameters and rf voltage profile for the synchrotron.

The equations of motion including space charge forces are derived in a Hamiltonian form. We assume that there is a synchronous particle that remains in the equilibrium orbit and whose energy is denoted by E_s. The Hamiltonian for a particle of energy E and phase Φ is:

$$H = \frac{h\eta_s\omega_s^2}{\beta_s^2 E_s}W^2 + \frac{eV}{2\pi}(cos\Phi + \Phi sin\Phi_s - cos\Phi_s - \Phi_s sin\Phi_s) - \frac{e^2 g_0 h^2}{4\pi\varepsilon_0\gamma_s^2 R}\lambda(\Phi), \quad (1)$$

where:
the subscript s refers to the synchronous particle,
$\lambda(\Phi)$ is the linear particle density,
ε_0 is the vacuum permittivity,
R is the average ring radius,
and g_0 is a capacitive geometrical factor $= 1 + 2ln(b/a)$, where a is the beam radius and b is the vacuum chamber radius. We define $W = (E - E_s)/\omega_s$, such that $dW \cdot d\Phi$ is conserved.

The differential equations derived from this Hamiltonian describe the time-evolution of a particle subject to an accelerating force that depends on the rf phase and to the space charge forces that act on the particle. These differential equations are solved numerically by using leapfrog difference equations that are suitable for rapid numerical calculations. The coordinates of each particle, W and Φ are advanced by a specified time-step, τ, according to:

$$W_{n+1/2} = W_{n-1/2} + \frac{eV_n\tau}{2\pi}(sin\Phi_n - sin\Phi_{s,n}) + \frac{e^2 g_0}{4\pi\varepsilon_0}\frac{h^2\tau}{R\gamma_{s,n}^2}(\frac{d\lambda(\Phi)}{d\Phi})_n, \quad (2)$$

$$\Phi_{n+1} = \Phi_n + h\tau(\frac{\eta_s\omega_s^2 W}{\beta_s^2 E_s})_{n+1/2} + \Phi_{s,n+1/2} - \Phi_{s,n-1/2}, \quad (3)$$

where the subscript n indicates that a quantity is evaluated at a time $t = n\tau$.

The values of the Φ coordinates are calculated at integer time-steps and the values of W, at half-integer time-steps. The last two terms in Eq.(3) account for the changes in Φ_s. These equations have first order simplicity but second-order accuracy, because the derivatives are evaluated at the mid-point of each interval. The numerical simulation of the injection, capture and acceleration processes follow an ensemble of macro-particles, whose initial coordinates in phase and energy are chosen according to a specified distribution.

The turn-by-turn injection process is simulated by randomly placing N_p/N_t macro-particles into the machine. Here, N_p is the total number of macro-particles, and N_t is the total number of injection turns. The particles are distributed uniformly in phase within the maximum and minimum values of the injected beam. The energy distribution follows a cosine distribution, where the base is equal to the maximum energy spread of the beam.

During injection, the time-step is equal to the revolution period. During the acceleration process, the time-step can be increased to reduce computer time, but must, of course, be kept much smaller than the synchrotron period, τ_s, or other relevant period of the motion. In the simulations, the time-step size is kept smaller than $\tau_s/30$.

The initial phase space coordinates for each particle are saved. The analysis of lost particles using these parameters permits the design of a more efficient injection scheme by depopulating the undesirable phase space. The vacuum chamber wall is represented by a momentum cutoff that depends on

the maximum betatron oscillation and dispersion function. Particles of equal, or higher, momenta than the cutoff are removed from the calculations, so as not to contribute to the space charge forces.

The variation of the capacitive geometrical factor during acceleration is also taken into account [6]. The geometrical factor depends on the ratio of the vacuum chamber radius and the beam radius. Since the latter decreases as the beam is accelerated, the ratio increases.

The space charge fields are calculated by using binning and data smoothing techniques that alleviate the statistical fluctuations introduced by the relatively small number of macro-particles used in the simulations.

The macro-particles are binned first into an appropriate number of bins. The number of bins must be chosen so that the average number of macro-particles per bin is not too small and the bin length not too large so as to reveal the bunch structure. A large number of bins reduces the bin occupancy, introducing higher frequency components. This can be seen in Figure 1, where 32 bins and 128 bins were used to estimate the derivative of the particle linear density distribution. A beam of length 180° and 10^4 macro particles were used in the simulation. The mean bin occupancy is 312 for the coarser binning and is 78 for the finer binning. For the latter, the ringing at the ends of the bunch that results from the Fourier series behaviour at a simple discontinuity (Gibbs phenomenon) is quite noticeable.

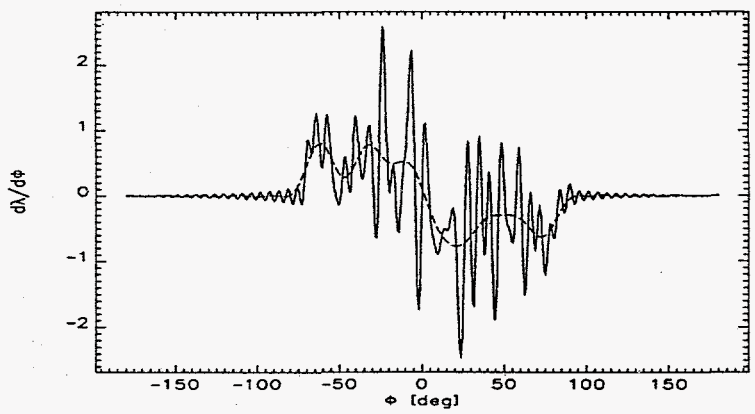

Figure 1: Gradient of the Linear Particle Density Distribution for a Beam of Length 180° Obtained with 32 Bins (Continuous Line) and 128 Bins (Dashed Line). The mean bin occupancy is 312 for the coarse binning and 78 for the finer binning.

The projected phase distribution is binned by the cloud-in-cell method [5]. For each particle, a weighted contribution is assigned to the two closest grid points, according to how far the particle is from these points.

The data is then fast-Fourier-transformed and convolved with a $sink/k$

kernel, where k is a harmonic number. This smoothens the binned density and provides a finer grid, from which the fields can be obtained by interpolation.

Finally, the Fourier components are multiplied by a Lanczos convergence factor:

$$\frac{sin\pi k}{k_c}/\frac{\pi k}{k_c},$$

where k_c is a cutoff harmonic number. The filtering process eliminates the ringing at the ends of the bunch, but has the disadvantage of introducing an overestimation of the density at the ends of the bunch and an underestimation of its peak. Figure 2 shows the linear particle density distributions from the example used in Figure 1 obtained after application of the same kernel interpolation but with cutoff harmonics of 9 and 17. The coarsely-binned data is obtained by using 32 bins and the interpolated data is obtained with 512 bins. As shown in the figure, the cutoff at the 9^{th} harmonic underestimates the peak of the distribution by 8% when compared with the peak of the distribution obtained from the 32-binned unfiltered data. The same cutoff overestimates the density at the ends of the bunch by 10%.

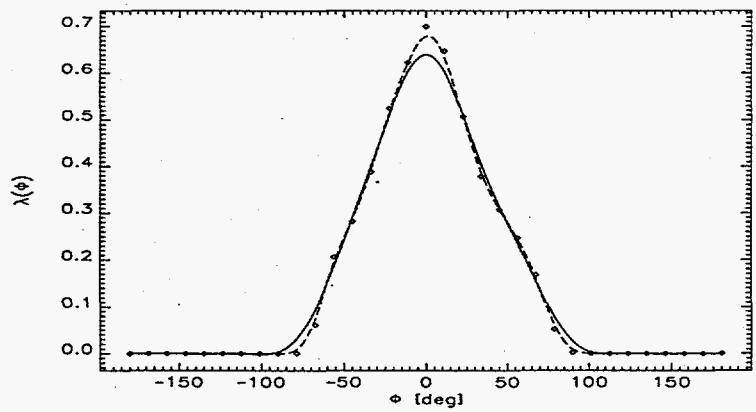

Figure 2: Linear Particle Density Distribution Obtained by Using Different Filter Cutoff Frequencies. The continuous line represents the density from a 9^{th} harmonic cutoff and the dotted line that from a 17^{th} harmonic cutoff. The squares represent the data before smoothening and filtering is applied.

The choice of the number of bins and cutoff frequency is based on an "optimal" filter method that gives the best estimate of the actual standard probability distribution from the computed density of the simulation particles [7].

Space Charge Issues in the 2-GeV Synchrotron

The accelerator system of the 1-MW source consists of an injector linac and a rapid cycling synchrotron (RCS). The 400-MeV linac delivers H^- ions to RCS, where they are injected after stripping by a thin carbon foil. RCS accelerates the beam from 400 MeV to 2 GeV and its rf system is operated with a harmonic number equal to one. The rf frequency varies from 1.1 MHz to 1.5 MHz. The synchrotron magnets are powered by a dual-frequency resonant circuit that excites the magnets at 20 Hz and de-excites them at 60 Hz, resulting in an effective rate of 30 Hz and a reduction of 1/3 in the required peak rf voltage value. The ring circumference is 190.4 m and the synchrotron fits in the former Zero Gradient Synchrotron (ZGS) enclosure. A layout of the accelerator system is shown in Figure 3.

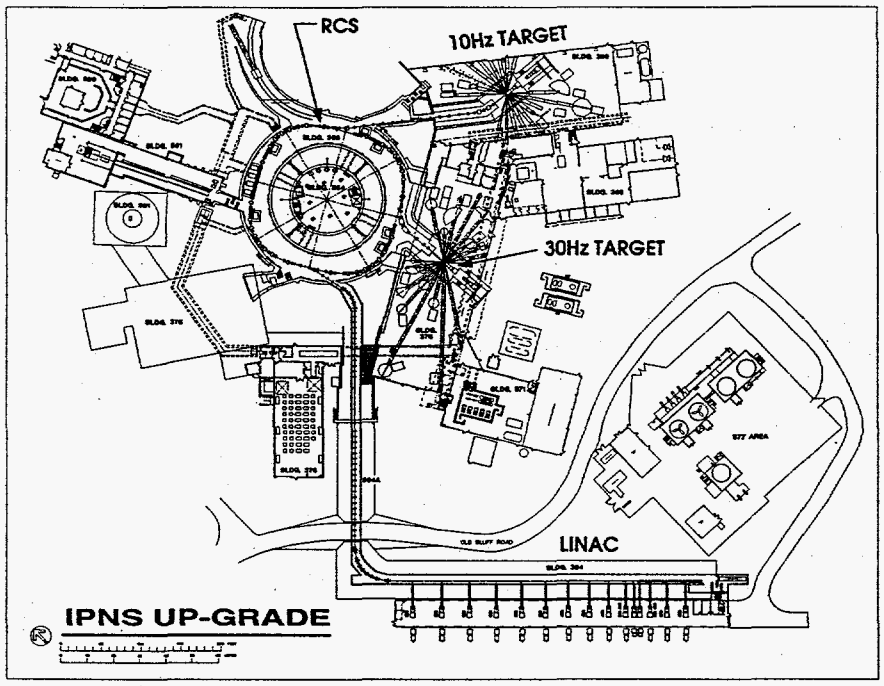

Figure 3: Schematic Layout of the IPNS Upgrade.

The space charge self-fields in the longitudinal direction vary as the inverse of the energy squared. In RCS, γ varies from 1.4 to 3.1 and the space charge self-fields affect the whole machine cycle. The fields change the beam dynamics and distort the rf bucket, thus enhancing the probability of beam losses. Since the main goal of the rf program design was to minimize losses, space charge effects in the synchrotron were analyzed in detail.

Some of the issues related to the prevention of beam losses in RCS are, at injection, choice of the injected-beam parameters and minimum initial bucket necessary to contain the beam while avoiding excessive dilution. During the injection period, the rf voltage must be increased to overcome the space-charge-induced bucket area reduction. During acceleration, the voltage needs to provide sufficient rf linear restoring force and the beam needs to have large momentum spread to prevent the microwave instability. During the whole cycle, the impedance due the space-charge self-fields must be minimized. In the following, we examine these issues separately.

The linac beam macro pulse is injected into a waiting bucket of RCS. Injection occurs in 0.5 msec, or 561 turns, under a flatbottom guide field. The choice of the initial particle distribution in phase space is guided by the requirements of high capture efficiency and longitudinal stability. The first requirement determines how much the linac macro pulse has to be chopped, since adiabatic capture is not pratical in RCS. The second requirement determines the bunch area of the beam. The simulation studies indicated that the best capture efficiency is obtained by discarding 25% of the linac beam and that the microwave instability is avoided when the bunch area after injection is 7.3 eV sec. Allowing a dilution factor of about two, an injected beam area of 3.3 eV sec satisfies the requirement. This area implies, in turn, that the the energy spread of the injected beam be equal to $\pm$ 2.5 MeV.

An important consideration in the studies was to avoid the need for large values of the rf voltage. The initial voltage was chosen so as to provide a bucket area sufficient to contain the incoming beam but not so large as to allow excessive dilution and the need for high rf voltage values at later times. The minimum voltage required to contain the beam injected with an energy spread of $\pm$2.5 MeV, cut by 25%, is 40 kV. Figure 4 depicts the bucket formed by this voltage and the particle distribution of the first injected turn. The voltage provides the needed bucket height at the edges of injected the bunch, as shown in the figure.

The rf voltage was raised rapidly during injection to avoid deleterious bucket area reduction caused by the increasing particle density as multiple turns are accumulated in the ring. In Figure 5(a) we show the phase space distribution at the end of injection, obtained by maintaining the voltage constant at 40 kV during the injection period. The initial bucket area of 7.0 eV sec is adequate to contain the injected beam of $\Delta E = \pm$ 2.5 MeV and $\Delta\Phi = \pm$ 135° as it undergoes synchrotron oscillations, but not enough to account for the bucket area reduction caused by the space charge forces. The bucket is 100% full and particles spill out of the bucket as it shortens during acceleration. For comparison, Figure 5(b) shows the phase space distribution at the end of injection when the rf voltage is raised by 43%, from 40 kV to 70 kV. In this case, the bucket area is 9.0 eV sec and the particles remain in the bucket

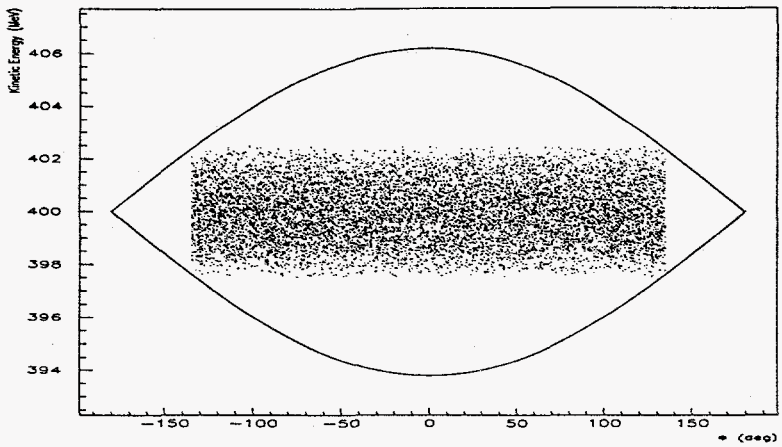

Figure 4: Bucket and Phase Space Distribution of the First Injected Turn in RCS.

as it is accelerated.

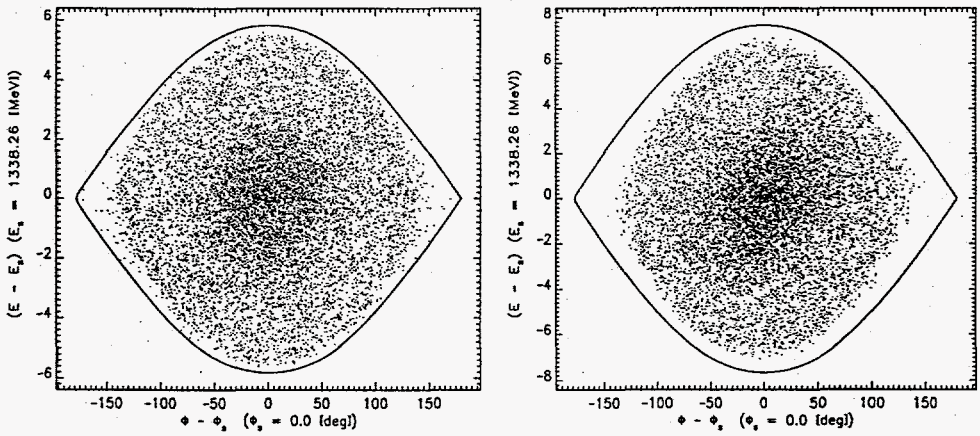

Figure 5: Particle Distribution at the End of Injection when (a) the Rf Voltage Is Maintained Constant During Injection and (b) the Rf Voltage Is Increased by 43%. Note the different scales used in the plots.

During the early stages of acceleration, the space charge forces in RCS are large enough to cause strong defocussing. An example of loss of focussing is shown in Figure 6(a). The figure depicts the instantaneous energy gain per turn at 1 msec of acceleration of a beam of initial energy spread $\pm$ 1.0 MeV chopped at 34% and injected into a 4.5 eV sec bucket. In the figure, the dashed line represents the energy gain due to the space charge, the short-dashed, that due to the rf voltage and the continuous line depicts the sum total of the energy gains. The acceleration provided by the rf is overcome

by the deceleration caused by the space charge, as indicated by the negative slope of the total energy gain near the synchronous phase. Figure 6(b) shows the bucket and the phase space distribution of the beam at 1 msec, where the bucket distortion is clearly seen.

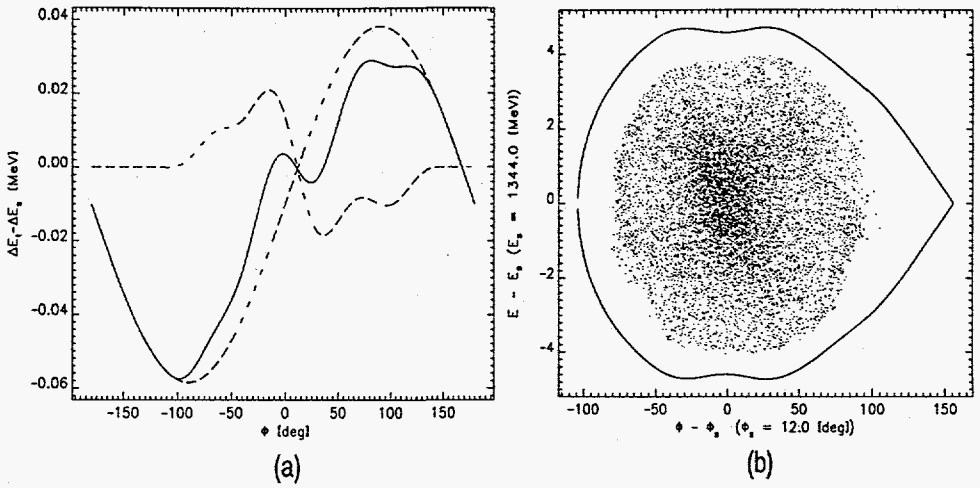

Figure 6: (a) Instantaneous Energy gain per Turn at 1 msec of Acceleration in RCS. The dashed line depicts the energy gain per turn due to the space charge alone, the short-dashed line represents the gain due to the rf voltage alone, and the continuous line is the sum total of the energy gains. (b) Bucket and Phase Space Distribution of the Beam whose Energy Gain per Turn is Shown in (a).

In general, loss of focussing may not be a concern, provided the bucket area is large compared to the bunch area and the beam is well matched to the bucket. In our studies, we opted for an adequate but not large bucket area in the ealier stages of acceleration while maintaining a well focussed beam.

Another factor that affects the longitudinal dynamics is the tune depression introduced by the space charge. In the presence of space charge, the synchrotron frequency does not decrease continuously with amplitude, as in the no-space-charge case. This can be seen as follows. The synchrotron frequency in presence of space charge produced by a beam of a given length can be estimated by the usual computation of the area under the Hamiltonian contour between two turning points of the motion:

$$\tau = \frac{1}{f_s} = 2\int_{\Phi_1}^{\Phi_2} \{2B[\Lambda(\Phi_2) - \Lambda(\Phi) + \frac{eV}{2\pi}(cos\Phi + \Phi sin\Phi_s - cos\Phi_2 - \Phi_2 sin\Phi_s)]\}^{-1/2} d\Phi, \quad (4)$$

where:
τ and f_s are the synchrotron period and frequency, respectively;

Φ is the rf phase; Φ_s is the synchronous phase;
Φ_1 and Φ_2 are the turning points of motion;
Λ is the space charge potential;
V is the peak rf voltage; and the constant

$$B = -\frac{h\eta\omega_s^2}{\beta_s^2 E_s},$$

with h the harmonic number, ω_s the angular revolution frequency, E_s the synchronous energy, β_s and γ_s the relativistic factors, and $\eta = 1/\gamma_t^2 - 1/\gamma_s^2$. γ_t is the transition energy. The contribution due to the space charge potential is given by the first two terms in the integrand of Equation (4).

In Figure 7(a) the synchrotron frequency is plotted as a function of amplitude for a bunch of 79° half phase spread, at the mid-point of the acceleration cycle in RCS.

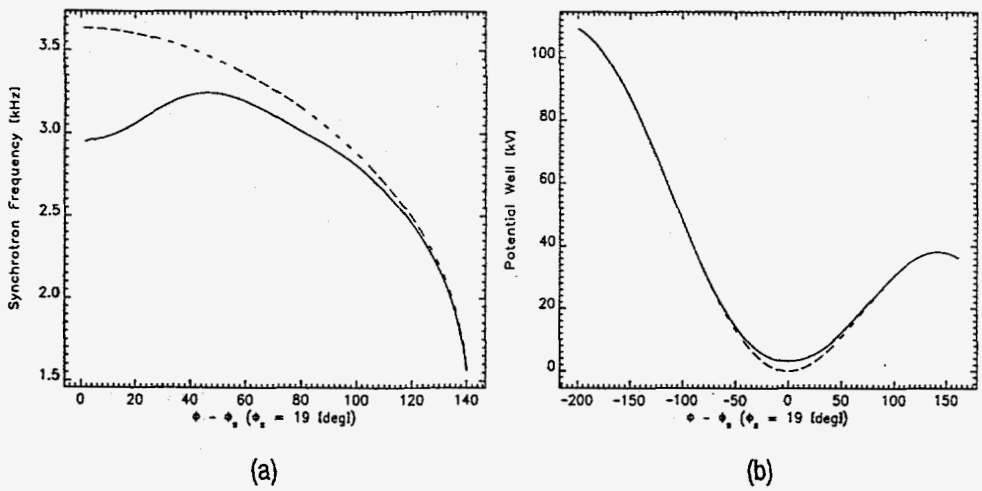

Figure 7: (a) Synchrotron Frequency as a Function of Amplitude, for a Beam of $\pm 79°$ Phase at t=12.5 msec of the Acceleration Cycle in RCS. The continuous line depicts the synchrotron frequency including space charge. The synchrotron frequency without space charge is represented by the dashed line. (b) Potential Well Including Space Charge (continuous line) and Without Space Charge (dotted line).

In the figure, the frequency variation calculated without the space charge contribution is also shown, for comparison. The corresponding potential distributions (with and without space charge) are plotted in Figure 7(b). Figure 7(a) shows that when the space charge potential is included, the particles near the synchronous phase have the largest frequency depression from the bare frequency, about 21%. As the particle density decreases near the end of the bunch, the depression decreases and tends asymptotically to zero towards the unstable fixed point.

During the acceleration cycle, the beam is kept above the microwave instability threshold by maintaining a large momentum spread. Longitudinal instability thresholds were obtained from the estimated coupling impedances [1]. The contribution to the longitudinal impedance from space charge dominates in RCS, where it is -220j ohms at injection energy and -50j ohms at extraction energy. RCS operates below the transition energy, thus the longitudinal microwave instability is not expected to occur unless there is a large resistive component. However, a conservative approach was adopted to ensure that the momentum spread is sufficient to satisfy the Keil-Schnell (KS) stability criterion, which is given by [8]:

$$|\frac{Z}{n}| \leq \frac{F|\eta|\beta^2 E/e}{I_{pk}}(\frac{\Delta p_{fwhm}}{p})^2 \tag{5}$$

Studies were performed to choose an rf voltage profile that provides adequate bucket area and momentum spread. Tracking studies show that the RCS beam remains in the stable region defined by the KS criterion over the duration of the acceleration cycle [9]. Figure 8 depicts the momentum spread of the beam obtained from tracking together with the longitudinal instability threshold according to the K-S criterion.

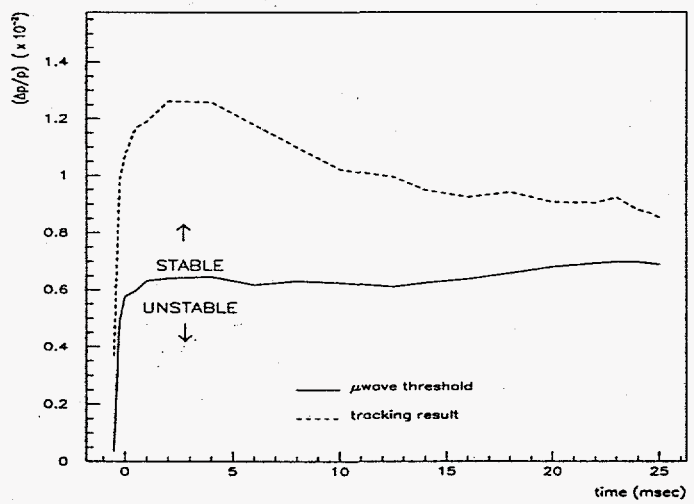

Figure 8: Longitudinal Instability Threshold and Momentum Spread of the Beam in RCS Obtained from Tracking Simulations.

The contribution to the longitudinal impedance from the space charge self-fields dominates in RCS. To minimize the space charge self-field impedance, the ceramic vacuum chamber is constructed with a special rf shield, such as that used at the ISIS facility of Rutherford-Appleton Laboratory [10]. The

shield follows the beam envelope at an aperture equal to the beam-stay-clear (BSC), defined as twice the emittance and the $\pm 1\%$ momentum spread of the injected beam. This reduces the longitudinal space charge impedance by 30% at injection and 20% at extraction.

Simulation studies addressing the aforementioned issues lead to the rf voltage profile and beam parameters for RCS that minimized the instabilities and beam losses. The rf voltage program and the time variation of the bucket and bunch areas in are shown in Figures 9 and 10, respectively. In the figures, t=0 indicates the start of the acceleration clock. The initial voltage is 40 kV, which is the minimum necessary to contain the beam injected with an energy spread of ± 2.5 MeV, cut by 25%. The bucket area is 7 eV sec and the bunch area is 3.4 eV sec. During the injection period, the voltage is raised from 40 kV to 70 kV to overcome bucket area reductions due to space charges. At the end of injection, the bucket and the bunch area are 9.0 eV sec and 7.3 eV sec, respectively. From the end of injection to 7.5 msec the voltage is designed to mantain a constant bucket area of 9.0 eV sec. The voltage reaches a maximum of 169 kV at 7.5 msec. For the remaining part of the cycle the energy spread of the beam is controlled by manipulating the bucket area. The voltage is kept constant from 7.5 msec to 12.5 msec, while the bucket area grows from 9.0 to 11.3 eV sec. After 12.5 msec, the voltage is decreased from 169 kV to 114 kV. The rf voltage is kept high during the later part of the cycle so as to provide a high enough synchrotron frequency that the particles in the bunch can follow the rapidly changing synchronous phase.

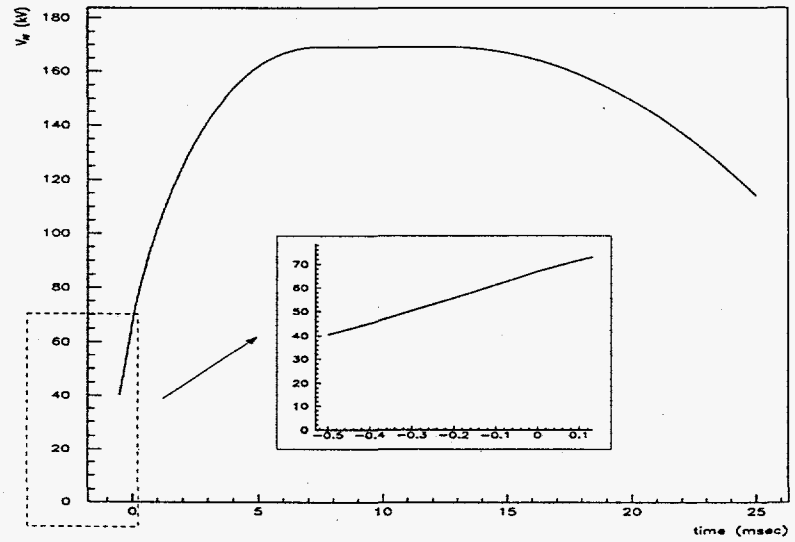

Figure 9: Rf Voltage Program for the Injection and Acceleration Cycles in RCS. The beginning of the acceleration clock starts at t=0.

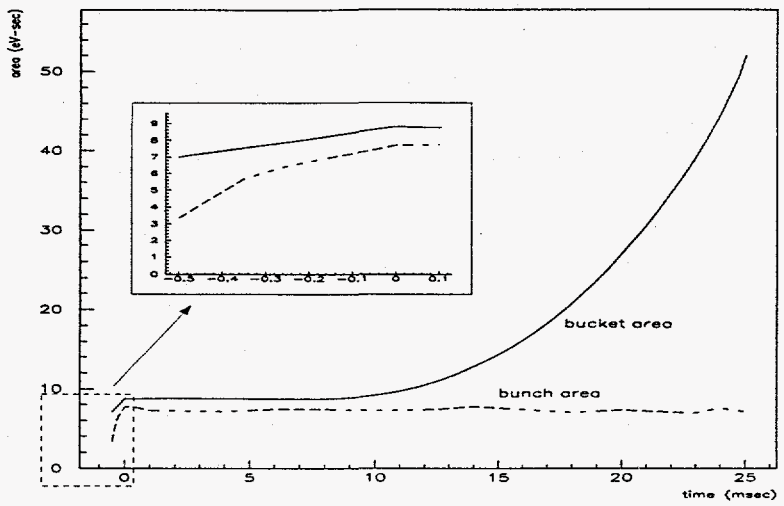

Figure 10: Bucket and Bunch Areas, Obtained from the Simulations under the rf Voltage Program Shown in Figure 9.

Space Charge Issues in the 10-GeV Synchrotron

The 10-GeV synchrotron (RCS-II) uses the 2-GeV synchrotron as its injector. In this case, the RCS rf system is run with a harmonic number equal to two, to provide two bunches for RCS-II. The circumference ratio between the 5-MW ring and the 1-MW ring is four. The RCS bunches at 3 MHz are transferred into waiting buckets of the 6-MHz RCS-II rf system which operates with a harmonic number of 16. RCS-II magnet are powered by a dual-frequency resonant circuit similar to the RCS circuit.

In RCS-II, the beam energy is high (γ varies from 3.1 to 11.7). However, space charge effects cannot be neglected in this machine, especially at injection and at extraction. At injection, space charge fields affect the matching between the incoming beam from RCS and the RCS-II waiting bucket. At extraction, the bunch length is short, about 22 nsec long, causing a high peak current.

The two bunches from RCS are injected into two buckets of RCS-II which are separated by an empty bucket. The bunch-to-bucket transfer between RCS and RCS-II is done by the following algorithm. The rf voltage at extraction of the 2-GeV beam determines the energy spread, ΔE, and bunch length, Δt, of the bunch. The energy spread and bunch length of the incoming beam are matched to a phase space area in the waiting bucket determined by the Hamiltonian contour that has the same ΔE and Δt. This determines the required initial voltage and the waiting bucket area. Figure 11(a) shows the rf bucket and the bunch population in RCS at extraction and Figure 11(b)

shows the bunch injected into the waiting bucket of RCS-II. The dashed line in Figure 11(b) represents the Hamiltonian contour whose height, ΔE, and whose enclosed area are equal to those of the injected beam.

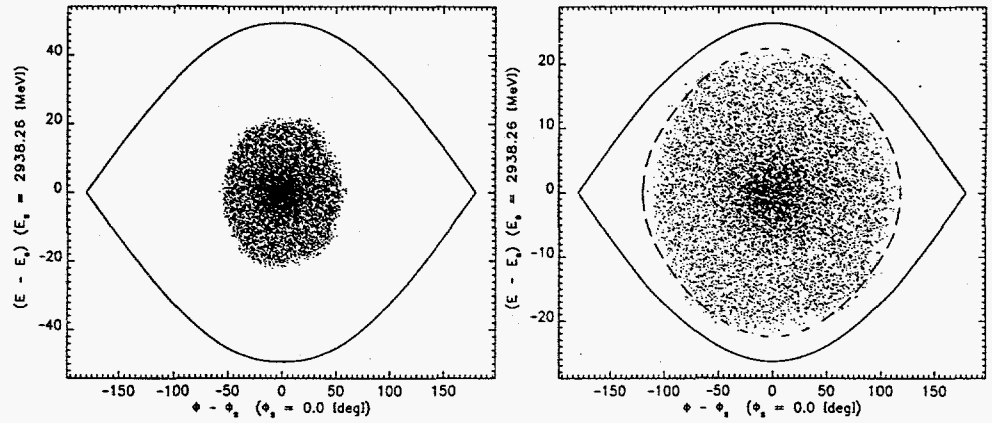

Figure 11: (a) Rf Bucket and Particle Distribution at Extraction in RCS. The single bunch area is 3.7 eV sec. (b) Rf Bucket and Phase Space Distribution at Injection in RCS-II. The dotted line indicates the contour enclosing an area of 3.7 eV sec.

Neglect of the space charge potential in the calculation of the Hamiltonian contour leads to underestimation of the necessary bucket area at injection and to consequent dilution of the beam as it is accelerated, due to mismatching. This can be seen in Figure 12(a), where we plot the phase space distribution of the beam at 6 msec into the acceleration cycle. In this case, the space charge contributions were not included in the bunch-to-bucket-transfer algorithm described above. The figure shows considerable dilution of the beam. For comparison, Figure 12(b) depicts the beam also at 6 msec, when the space charge contributions were included.

In RCS-II, the space charge impedance is smaller than in RCS by a factor of 5 at injection and 10 at extraction. The peak current in RCS-II is 160 A at injection and less than 800 A at extraction. The voltage has to be kept high at the later stages of acceleration not only to provide a high enough synchrotron frequency, as in RCS, but also to avoid collapse of the bucket due to the high peak current.

Figure 13 shows the rf voltage and bucket and bunch areas from injection to extraction in RCS-II obtained from simulations. The initial voltage determined by the matching procedure aforementioned is 0.7 MV and the corresponding single bucket area is 5.8 eV sec. This area is maintained at this initial value for the first 8.0 msec, when the voltage reaches a maximum value of 1.9 MV. The voltage is decreased to 1.7 MV at extraction.For the latter part of the cycle, the voltage is maintained high as explained above. The rf program for RCS-II

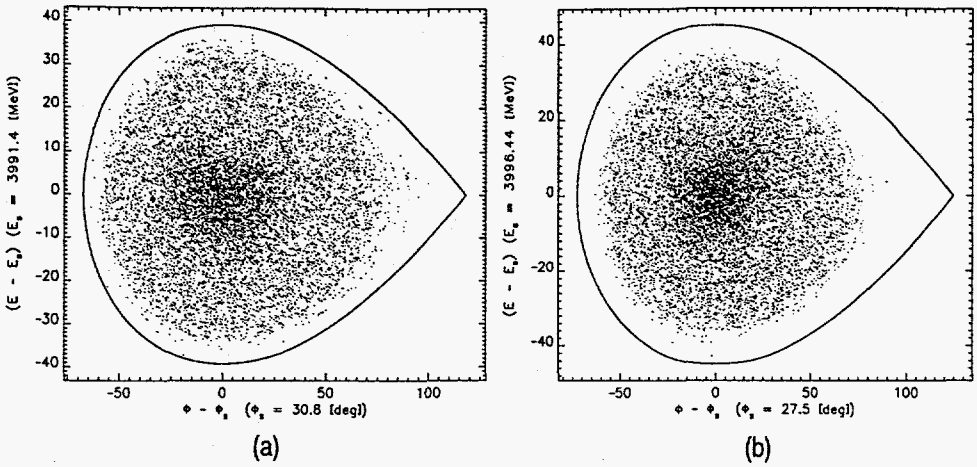

Figure 12: Phase Space Distribution of the Beam at 6 msec of the Acceleration Cycle in RCS-II when: (a) the Waiting Bucket Area Is Calculated without Space Charge and (b) the Waiting Bucket Area Is Calculated with Space Charge.

satisfies the no-loss criterion and satisfies the KS criterion through most of the acceleration.

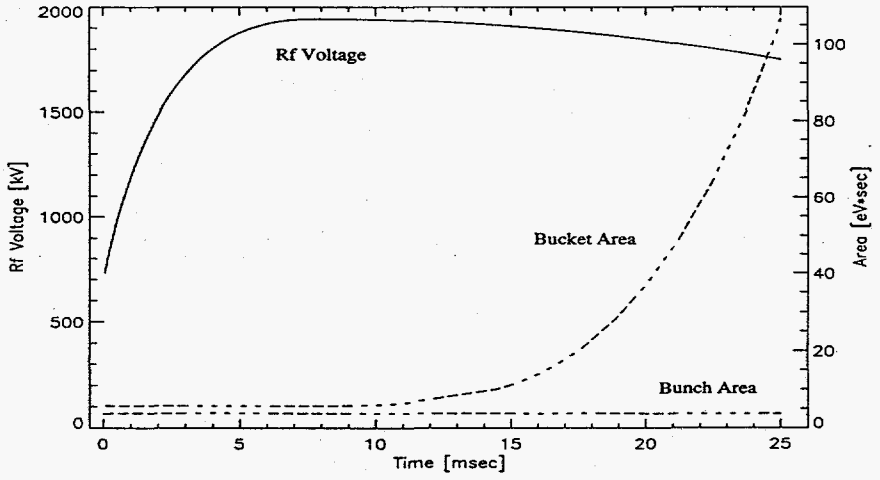

Figure 13: Rf Voltage Program for RCS-II, Showing the Time Evolution of the Bucket (solid line) and Bunch (dotted line) Over the Complete Cycle.

Summary

The space charge self-fields are large in the synchrotrons of a 1-MW and a 5-MW spallation neutron sources designed to deliver 1.04×10^{14} protons per pulse at a repetition rate of 30 Hz. Longitudinal space charge effects were examined

in detail by tracking simulations and means to circumvent these effects were investigated. The tracking studies were used to formulate rf voltage profiles and beam parameters that facilitate keeping beam losses in both synchrotrons to radiation levels that allow hands-on maintainance.

References

[1] "IPNS Upgrade – A Feasibility Study," ANL Report ANL-95/13 (April, 1995).

[2] Y. Cho, et. al. "A 10-GeV, 5-MW Proton Source for a Pulsed Spallation Source," *Proc. of the 13th Meeting of the Int'l. Collaboration on Advanced Neutron Sources*, PSI, Villigen, to be published (Oct. 11-14, 1995).

[3] K. R. Symon, "Synchrotron Motion with Space Charge," ANL Report NSA-94-3 (April 4, 1994).

[4] Y. Cho, E. Lessner and K. Symon, "Injection and Capture Simulations for a High Intensity Proton Synchrotron," *Proc. of the European Particle Accelerator Conference*, London, page 1228 (1994).

[5] C. K. Bird and A. B. Langdon, "Plasma Physics Via Computer Simulations," *Adam Higler*, Bristol, England, 1991, page 19.

[6] K. C. Harkay, "Transverse Beam Size and Ratio (b/a) in Space Charge Geometry Factor for RCS-II," ANL Report NSA-94-1 (April 4, 1994).

[7] K. R. Symon, "Optimal Filtering in Space Charge Simulations," ANL Report NSA-94-4 (May 24,1994).

[8] V. K. Neil and A. M. Sessler, "Longitudinal Resistive Instabilities of Intense Coasting Beams in Particle Accelerators," Rev. Sci. Instrum. **36**(4), 429 (1965).

[9] K. Harkay, Y. Cho and E. Lessner, "Longitudinal Instability Analysis for the IPNS Upgrade," *Proc. of the 1995 Particle Accelerator Conference*, Dallas, Texas, to be published (May 1995).

[10] G. H. Rees, "Status Report on ISIS," *Proc. of the IEEE Particle Accelerator Conference*, London, page 1228 (1994).